Surface Drift and Dispersion in a Multiply Connected Fjord System

Hauke Blanken, Charles Hannah, Jody M. Klymak, & Tamás Juhász

February 2020

JGR Oceans

RESEARCH ARTICLE
10.1029/2019JC015425

Special Section:
Coastal hydrology and oceanography

Surface Drift and Dispersion in a Multiply Connected Fjord System

Hauke Blanken[1,2], Charles Hannah[1], Jody, M. Klymak[2], and Tamás Juhász[1]

[1]Institute of Ocean Sciences, Department of Fisheries and Oceans Canada, Sidney, British Columbia, Canada, [2]School of Earth and Ocean Sciences, University of Victoria, Victoria, British Columbia, Canada

Abstract The deployment of 206 surface drifters over 3 years in a fjord system in northern British Columbia allows examination of drift and dispersion in complex coastal regions on time scales up to 10 days. The surface drift is found to be seasonally variable, with stronger dispersion and outflows in the spring and fall, and negligible outflow in the summer. Dispersion at time scales less than 10 hr is well described by fractional Brownian motion, where the drifter tracks exhibit fractal characteristics with a dimension of 1.34 over scales of 2 to 13 km. Drifters are found to reach less energetic nearshore regions within 12–15 hr, which slows along-channel dispersion. The comparison of the drifter statistics (from 2014–2016) with observations of the spatial distribution of oil sheen following an oil spill in 2006 shows that the drifter results provide a reasonable proxy for oil drift in this area. A statistical model for the extent of along-channel transport of spilled oil is proposed for use in planning emergency response activities in the area.

Plain Language Summary This paper is an analysis of the movement of 206 surface drifting buoys (drifters), which were released in the Kitimat fjord system in northwestern British Columbia between 2014 and 2016. This fills a knowledge gap concerning drift of objects at the ocean surface in narrow fjord systems over times longer than 1 day. Drift is toward the ocean on average and stronger in the spring and fall than in the summer. Drifters move approximately twice as fast near midchannel than they do near the shorelines and are found to come in close proximity of the shoreline within 12–15 hr of being released. Consequently, this cross-channel movement slows drift along the channel. Comparison with observations of sheening from a previous oil spill in the study region suggests that the drifters are an adequate proxy for spilled oil. A statistical model for the maximum likely extents of oil spills in the fjord system after times up to 10 days is proposed.

Key Points:
- Analysis of ocean surface dynamics in a multiply connected fjord system from 3 years of drifter data
- Over time scales longer than 15 hr interaction between the drifters and channel walls restrict along-channel dispersion
- The drifters are an adequate proxy for oil and results can be used for spill response planning

Supporting Information:
- Supporting Information S1

Correspondence to:
H. Blanken,
hauke.blanken@dfo-mpo.gc.ca

Citation:
Blanken, H., Hannah, C., Klymak, J. M., & Juhász, T. (2020). Surface drift and dispersion in a multiply connected fjord system. *Journal of Geophysical Research: Oceans*, *125*, e2019JC015425. https://doi.org/10.1029/2019JC015425

Received 27 JUN 2019
Accepted 27 JAN 2020
Accepted article online 3 FEB 2020

1. Introduction

Increasing development of coastal regions requires improved knowledge of complex local oceanographic processes in order to support development while protecting ecosystems in the face of increased shipping and other human activity. Understanding of drift and dispersion at the ocean surface is a key requirement for these endeavors, to predict the transport and dispersion of buoyant contaminants such as oil (cf. Fingas, 2011; Hackett et al., 2006), larval organisms and other biological material (Röhrs et al., 2014), and targets of search and rescue operations (Breivik & Allen, 2008; Daniel et al., 2002; Davidson et al., 2009).

Surface circulation in coastal fjords is driven by tidal currents, wind forcing, and estuarine circulation induced by fresh river inputs and terrestrial runoff (Farmer & Freeland, 1983; Thomson, 1981). The combination of these forcings and the associated stratification often results in complex flow patterns with significant spatial and temporal variability. When considering the drift of objects at the ocean surface, wave-induced circulation and direct wind forcing acting on exposed parts of the object must also be taken into account (Röhrs et al., 2012).

Freely drifting buoys at the ocean surface (drifters) can reveal insights into the dynamics and statistics of ocean surface flow. Certain types of drifters can also be used as a direct proxy for the transport of spilled oil (Fingas, 2011), though this is not guaranteed as behavior may vary significantly between drifters that are drogued at different depths within the upper meter of the water column (Röhrs & Christensen, 2015). Data

from surface drifters are also a valuable resource for validation of numerical models, which are often used to estimate surface circulation in operational applications.

Drifter studies in the open ocean and on continental shelves are well documented, both for surface circulation (cf. Crawford et al., 1999; Davis, 1985a, 1985b; Poje et al., 2014) and deeper circulation using drogues (cf. Freeland et al., 1975; Niiler & Paduan, 1995; Poulain & Niiler, 1989; Rupolo et al., 1996). These studies infer mean circulation patterns and speeds as well as dispersion characteristics, both for the absolute dispersion of the drifters as well as the relative separation between them. They make use of significant amounts of data and long time series collected by drifters well away from the coastlines. In areas closer to the shoreline long time series are more difficult to collect as drifters often ground on the shoreline (Pawlowicz et al., 2019; Swick & MacMahan, 2011).

Drifter data from fjords and other topographically restricted coastal regions is usually limited to deployments of 24 hr or less (cf. de Young & Sanderson, 1995; Nairn & Kawase, 2002; Spencer et al., 2014; Spydell et al., 2007, 2015; Tseng, 2002; St-Onge-Drouin et al., 2014). These studies provide useful estimates of mean drift and dispersion for time scales on the order of a tidal cycle, but do not provide information on longer time scales. Pawlowicz et al. (2019) report on statistics from expendable drifters released in the Salish Sea, an inland sea in southern British Columbia, Canada. The lifetimes of their drifters sometimes exceeds 30 days, though they generally ground ashore within 3 days. However the Salish Sea is an estuarine system with a channel width that exceeds the internal Rossby radius of deformation appreciably, and therefore differs from the interconnected narrow fjords that characterize much of the coastline in northern regions of the world. Here we aim to address a gap in the literature by analyzing a set of longer drifter trajectories in a system of multiply connected, narrow coastal fjords.

Estimates of absolute dispersion from drifter data are often based on the theory of Taylor (1921), which considers one-dimensional dispersion in stationary, isotropic, and homogeneous turbulent flow. The theory has been extended to two-dimensional anisotropic applications and several drifter data sets have been described using this theory (Davis, 1985b; 1987; Poulain & Niiler, 1989; Spydell et al., 2007). The theory predicts that the drifters' displacement variance (which is a proxy for occupied area) will grow proportionally to time raised to the power of 2. In a fjord system, any dispersion model that is applied on length scales comparable to the channel widths should account for the fact that dispersion characteristics may vary significantly across the channel (Swick & MacMahan, 2011) and that boundaries may induce anomalous (non-Taylorian) dispersion (Artale et al., 1997; LaCasce, 2008).

An alternative dispersion model based on fractional Brownian motion (fBm) has produced good results over the length scales on which drifter trajectories exhibit a fractal character (100+ km in the open ocean) (Sanderson & Booth, 1991). FBm can be used to describe dispersion where persistent autocorrelations in the flow result in non-Taylorian behavior. It predicts displacement variance growth proportional to time raised to the power of 1.5 for a fractal dimension of 1.3. This fractal dimension has been repeatedly reported in drifter literature (Osborne et al., 1989; Sanderson et al., 1990; Sanderson & Booth, 1991). In this context the fractal dimension may be thought of as a measure of the portion of the available space that a drifter occupies. A fractal dimension of 2 implies pure Brownian motion which eventually fills a plane entirely, while a fractal dimension of 1 implies motion along a straight line (Sanderson & Booth, 1991). Fractional Brownian motion was used to describe drifter dispersion and residence time in a coastal embayment by de Young and Sanderson (1995) and has been used to model pollutant dispersion in coastal regions with some success (Addison et al., 1997; Guo et al., 2009).

In this paper we present a study of drifter data from the Kitimat fjord system in northwestern British Columbia, Canada, where 206 surface drifters were deployed between March 2014 and July 2016 (Page et al., 2019). Their tracks cover the study region well and allow us to derive general results about mean drift patterns and dispersion on time scales up to 10 days. This was not previously possible in narrow, interconnected fjord systems due to the short duration of drifter tracks. The observed along-channel dispersion pattern is then contextualized by analyzing the effects of cross-channel drift and interaction with the shoreline. We then investigate the general dynamics of the drifter motion further and provide evidence that the drifter tracks exhibit fractal characteristics. Finally, we confirm that the tracks of the observed drifters are an adequate proxy for spilled oil as they correspond well with observations of diesel sheen made after the passenger ferry *Queen of the North* sank in the study area in 2006. On this basis we propose a statistical model for the possible distance over which oil spills in the Kitimat fjord system may be transported within 10 days.

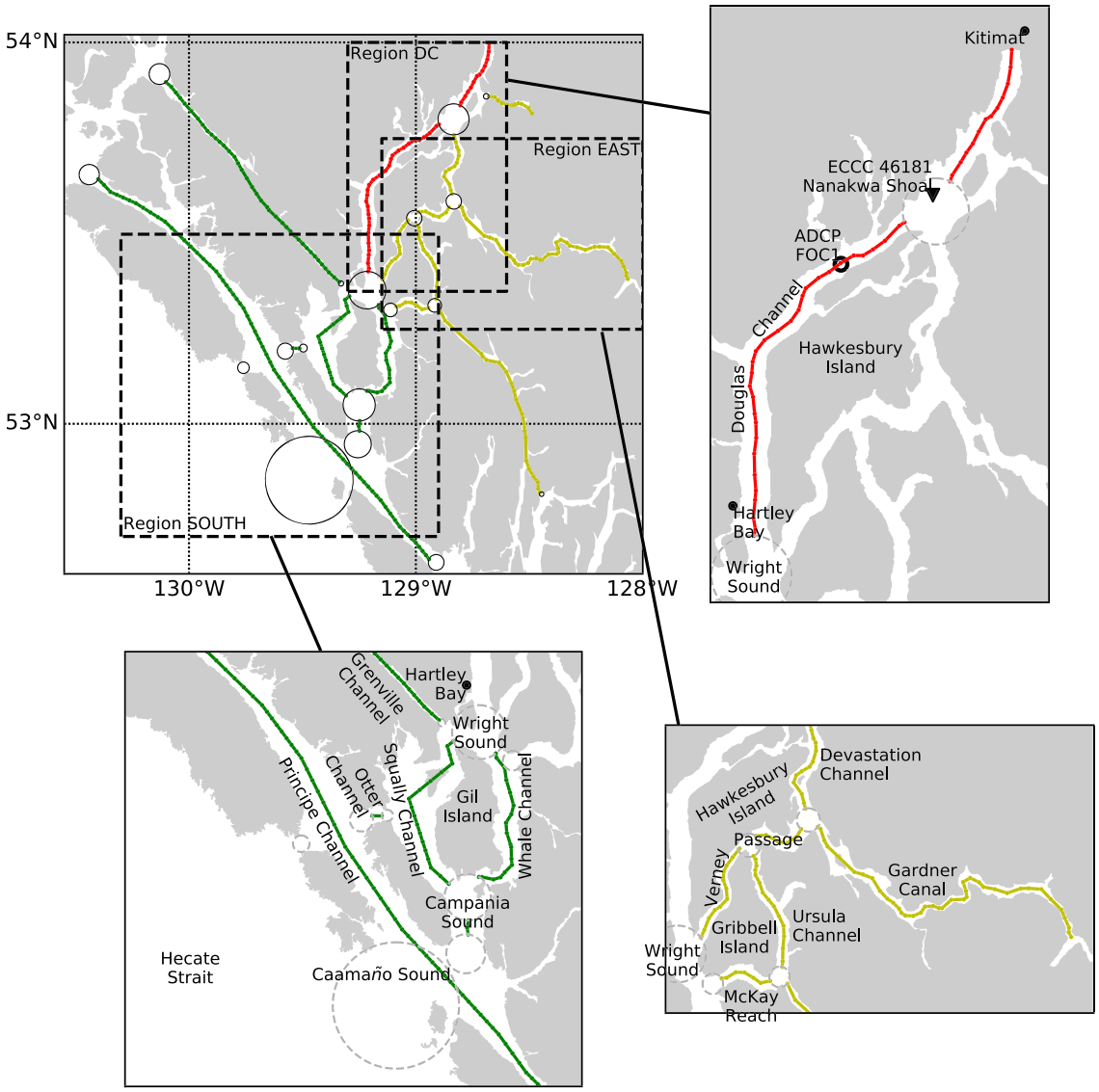

Figure 1. Map of the Kitimat fjord system showing subregions DC, EAST, and SOUTH, and grid system for analysis of along-channel dispersion. Channels in region DC are shown in red, region EAST in yellow, and region SOUTH in green.

2. Observations

2.1. Physical Setting

The Kitimat fjord system (Figure 1) is located in northwestern British Columbia, Canada, and spans from the coastal waters of Hecate Strait to the town of Kitimat, approximately 140 km inland. Douglas Channel is the main channel in the system and reaches from Kitimat to the community of Hartley Bay, at the northern edge of Wright Sound. Here it splits into Squally Channel to the west and Whale Channel to the east. These channels eventually connect to Hecate Strait. When discussing regional differences within the system Douglas Channel will hereafter be referred to as DC, the smaller channels east of Douglas Channel as EAST, and the channels south of Wright Sound as SOUTH.

Surface flow in the fjords generally follows the outflow pattern expected in estuarine circulation (Macdonald et al., 1983; Wan et al., 2017; Webster, 1980). During the period July 2013 to July 2016 near—surface currents (depth 7 to 12 m) were measured at a number of locations in the system (Wright et al., 2015, 2016, 2017). These measurements indicate mean year-round seaward motion at a rate of 3–17 cm s^{-1} superimposed on RMS velocity fluctuations of 19–30 cm s^{-1}. Mean flows are directed along the channel axis, and

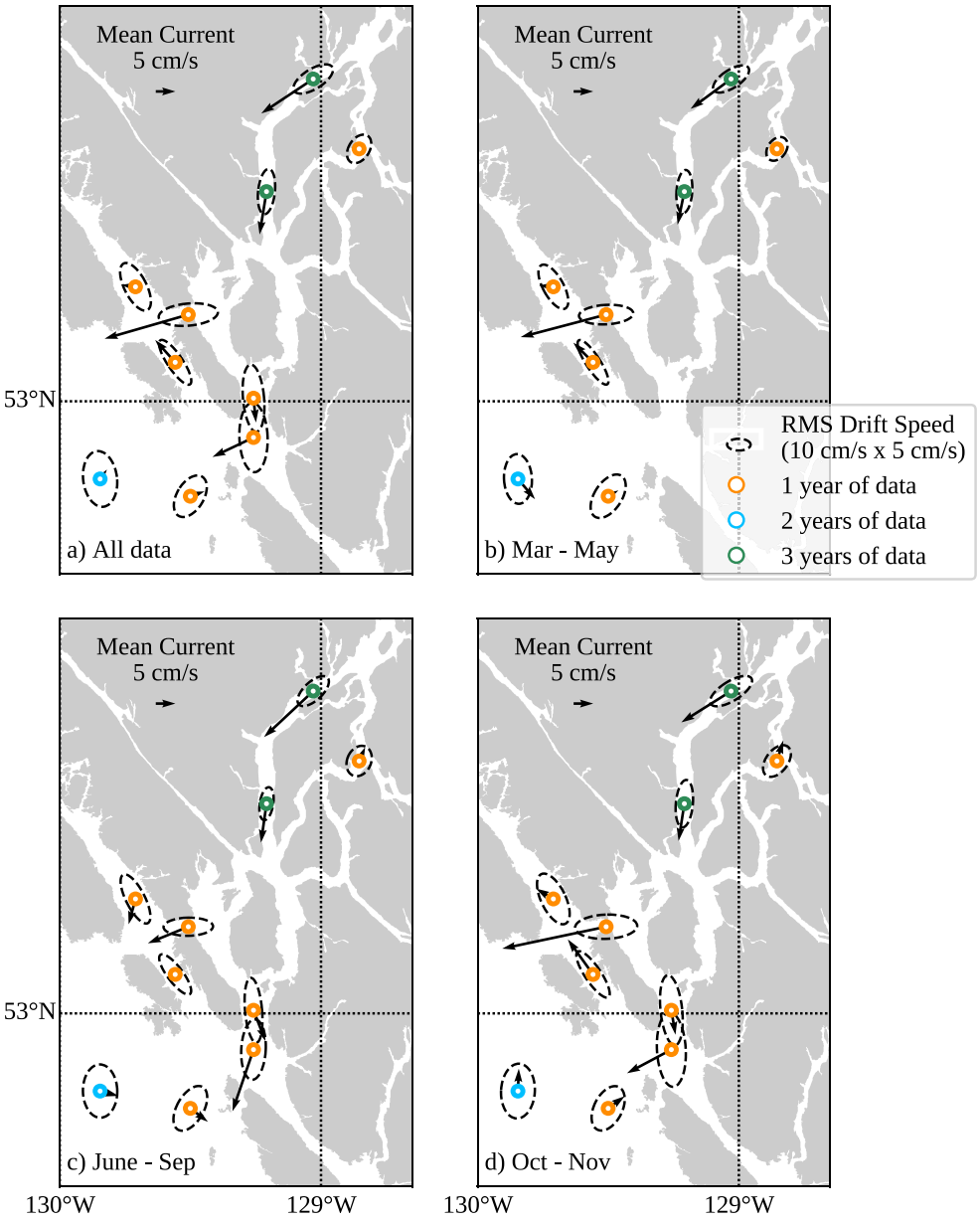

Figure 2. Mean (arrows) and RMS (ellipses) velocities recorded by acoustic Doppler current profilers deployed in the Kitimat fjord system between July 2013 and July 2016. Statistics are shown for the entire available record (a), as well as seasonal statistics separated into spring (b), summer (c), and fall (d). The record length at each location is indicated by the marker color.

cross-channel currents are weaker than along-channel currents, generally by more than 50% (Figure 2). This is in good agreement with previous current records from the region (Huggett & Wigen, 1983).

The M2 component dominates tidal currents, with a near-surface amplitude of 0.2 m s^{-1} (Webster, 1980). Tidal ellipses near the surface are not strictly rectilinear (Rabinovich et al., 2017), but the cross-channel tidal excursion is small (~500 m) compared to the width of the channels (~3–5 km).

The top ~10 m of the water column in the upper reaches of the fjord system are strongly stratified due to freshwater input from rivers and direct runoff, as indicated by measurements of temperature and salinity taken between 2013 and 2016 (supporting information Figure S1). Stratification increases throughout the year, as peak freshwater input occurs between May and August and surface heating increases until early fall. This strong stratification can result in increased wind influence on surface currents (Thomson, 1981). Wan et al. (2017) investigated the near-surface currents and found that 60%–70% of the subtidal variance in the

Figure 3. The final drifter design.

currents could be explained by a linear regression against wind speed. The wind-driven flow (~5% of the wind speed) is superimposed on an estuarine surface outflow of 14–23 cm s^{-1}.

Winds are generally variable in spring and fall, and up-channel on average in summer (supporting information Figure S2). Summertime up-channel wind-driven flow may counteract the estuarine surface outflow almost entirely (Wan et al., 2017). All wind data are based on measurements at a buoy near the northern end of Douglas Channel (ECCC 46181 Nanakwa Shoal on Figure 1). The strongest wind recorded during times that drifters were active is 15 m s^{-1} (30 knots). Based on the historical buoy record winds of this magnitude occur once every 15 years in the period April to October, but more than once per month in wintertime. Waves in the Kitimat fjord system are fetch-limited and generally small (<1 m with periods less than 5 s) (supporting information Figure S3).

A more detailed description of the ADCP and CTD data collected in the Kitimat fjord system between 2013 and 2016 is given in the supporting information and in Wright et al. (2015, 2016, 2017) and Wan et al. (2017). Further descriptions of the Kitimat fjord system are given by Webster (1980), Macdonald et al. (1983), and Shan et al. (2019).

2.2. Drifter Program

Novel, low-cost, surface circulation tracking drifters were developed as part of this study (Figures 3 and S4). Their shallow draft (375 mm) serves to mimic the behavior of objects drifting in the uppermost part of the ocean under the influence of winds, waves, and currents. The drifter's position is tracked using the motion-activated, commercially available SPOT asset tracking unit (SPOT LLC). The unit is attached to the top of the drifter by a stiff spring, to ensure frequent motion of the tracking unit even when the drifter is in calm water. Buoyancy is provided by a reinforced cylindrical cellulose sponge, and an array of cylindrical aluminum vanes serves to increase submerged surface area. In its final design the water surface is approximately 3–5 mm below the top of the sponge. This results in a 15:1 ratio of submerged to exposed cross-sectional area weighted by drag coefficient (following ; Niiler et al., 1995). The drifters are described in more detail in Page et al. (2019).

The drifter deployments were designed to maximize the seasonal and spatial coverage of the tracks. Drifters were deployed in groups of two to five throughout the study area in March, June, and October of 2014, March, July, and November of 2015, and May and July of 2016. In total 206 drifters were deployed within the Kitimat fjord system, and they collected a total of 2,741 drifter-days worth of data (spring: 991 drifter-days, summer: 1037 drifter-days, fall: 713 drifter-days). The longest track in the data set is 94.5 days long, recorded in March 2014. Some drifters traveled outside of the study region, but only the positional fixes recorded within the Kitimat fjord system are considered in the analysis. Analysis is performed for time scales up to 10 days, as few drifters remained freely drifting within the fjord system after this time. The drifters transmitted their position on irregular time intervals with an average of ~25 min once the drifter design had been optimized (Fall 2014 to Summer 2016).

3. Methods

3.1. Channel Coordinates

Drifter motion is decomposed into along-channel and cross-channel coordinates for analysis of long-term dispersion patterns. We only consider seaward (positive, toward Hecate Strait) and landward (negative, toward Kitimat) motion as we cannot statistically resolve the dispersion between individual channels. Drifter positions are mapped to a grid system defining along-channel direction throughout the study region (Figure 1). This system divides the region into 16 channels and 18 confluences. Each channel consists of waypoints along the centerline, which are spaced no more than 3 km apart (colored lines in Figure 1). Within channels, displacement associated with pairs of drifter positional fixes is determined by locating the closest

waypoint to each fix and projecting the displacement vector between the two fixes onto the down-channel direction (from waypoint to waypoint). If there are intermediate waypoints between those closest to the fixes the along-channel displacement is taken as the distance between the intermediate waypoints and the distance between the closest waypoint and the projection of the positional fix onto the along-channel axis.

At a confluence of two or more channels (black circles in Figure 1) the down-channel direction is determined based on the drifters proximity to the adjacent channels. If a drifter is close to a particular channel for at least 1 hr it is considered to be "in" that channel, and its motion is calculated using the channels closest down-channel direction. The radius of each confluence is chosen so that the confluence spans the entire width of the channel in every possible direction. If a confluence lies between two successive positional fixes the along-channel displacement through the confluence is considered to be the linear distance between the terminal points of the initial and final channel. If a drifter traverses more than one intermediate channel between two successive positional fixes (i.e., the drifter traversed more than two confluences) the drifter track is split between these two fixes, into two separate tracks.

We quantify the along-channel dispersion of drifters throughout the system by mapping the positional data to the grid system described above. Dispersion can be studied by considering time series of along-channel displacement, X, over a range of time lags τ.

$$\Delta X(\tau) = X(t+\tau) - X(t) \tag{1}$$

We assume $\Delta X(\tau)$ to be a property of the drifter track that is independent of initial time t, that is, statistically stationary. All nonoverlapping segments of a drifter track are therefore used in the analysis. For example, a 200-hr-long drifter track will yield 400 values of $\Delta X(\tau = 0.5$ hr), 200 values of $\Delta X(\tau = 1$ hr), etc.

The time-evolving mean, $\mu(\tau)$, and variance, $\sigma^2(\tau)$, of $\Delta X(\tau)$ can then be used to estimate the limits of displacement by using the 95% confidence intervals of a Gaussian distribution. This is a proxy for the area within which we expect to find 95% of the drifters, and will be extended for application to oil spill response in section 6. Mathematically, this can be expressed as follows:

$$\Delta X(\tau)_{\min/\max} = \mu(\tau) \pm 2\sqrt{\sigma^2(\tau)} \tag{2}$$

To study cross-channel motion, we define the drifters' proximity to the shoreline, d_{shore} to be the minimum distance between the drifter and the closest polygon in the GSHHS coastline database (Wessel & Smith, 1996). We further define the local channel width, w, as the minimum distance between the nearest point on a coastline polygon and the next closest polygon (which is the other side of the channel). We then derive the normalized cross-channel position, denoted χ, as

$$\chi = \frac{2d_{\text{shore}}}{w} \tag{3}$$

such that $\chi = 1$ refers to midchannel, and $\chi = 0$ refers to the shoreline.

3.2. Drift Velocity Statistics

We estimate velocities from the drifter positions by interpolating positions to even 15-min intervals using cubic splines, and then taking centered differences, with a forward (backward) difference at the start (end) of each track (Thomson & Emery, 2014). Points where the estimated drift velocity is less than 2 cm s^{-1} are discarded in order to reduce the effects of position uncertainty and to eliminate drifters that have grounded ashore. The uncertainty associated with positional fixes recorded by the SPOT GPS transmitter is estimated to be ~9 m (seeFigure S5). For velocity derived from two positional fixes recorded 15 min apart this results in a speed uncertainty of 0.02 m s^{-1} (= 2(9 m/900 s)).

Drift velocity statistics can be estimated in the Eulerian sense by binning points into subregions. Binning is done subjectively, with the aim to ensure adequate sample size in each bin while also minimizing the number of sharp changes in channel geometry within a subregion. No statistics are reported for subregions with less than 10 statistically independent samples of drift velocity.

To achieve statistical independence between sampled drift velocities we compute the mean Lagrangian integral time scale, T_i, from tracks in each subregion and only consider estimates separated by time intervals longer than $< T_i >$ (Swick & MacMahan, 2011). Subscripts i denote orthogonal components of velocity. T_i

is derived by integrating the mean normalized autocovariance function, considering times up to 25% of the length of the drifter track (Thomson & Emery, 2014). Tracks available for this analysis are generally short, as drifters frequently move between subregions or ground on the shoreline. Since the integration does not converge readily at the longest available lags we adopt the practice of integrating to the time of first zero-crossing, T_{i0} (Poulain & Niiler, 1989). The arithmetic mean of the integral time scale in the u and v (N-E coordinates) directions is used as T_i.

3.3. Fractional Brownian Motion

We consider fractional Brownian motion as a possible description of the single-particle dispersion statistics of the drifters on short space and time scales, following Sanderson and Booth (1991). A brief overview of the concepts that are relevant to the analysis in this paper are given. For a more thorough treatment of the topic the reader may refer to works such as Mandelbrot and Van Ness (1968); Molz et al. (1997), and Lilly et al. (2017).

Fractional Brownian motion (fBm) is a stochastic model built on ordinary Brownian motion with the additional feature that the motion increments are infinitely self-correlated, that is, the process has an infinite memory of its own history. Mathematically, it is equivalent to a moving average of incremental ordinary Brownian motion, in which previous increments are weighted by a time-dependent kernel (Mandelbrot & Van Ness, 1968). The resulting variance of particle displacements, x, at a time t after initial time t_0 can be written as

$$< [x(t_0 + t) - x(t_0)]^2 >= AV_H t^{2H} \tag{4}$$

Here H is related to the fractal dimension D of the two-dimensional drifter motion by $D = \min[1/H, 2]$, assuming isotropic statistics (Sanderson & Booth, 1991); A is an amplitude coefficient after Lilly et al. (2017); and V_H is the weighting kernel as defined by Mandelbrot and Van Ness (1968).

A surface drifter trajectory is restricted to a fractal dimension between a line ($D = 1$) and a plane ($D = 2$) which corresponds to the parameter space $1 > H > 0.5$. When $H = 0.5$ (and $D = 2$) the position variance grows linearly in time (equation (4)) and the motions will fill the two-dimensional space available to it if given enough time, whereas the trajectories from fBm will look increasingly like a line as H increases from 0.5 to 1 (Figure S6) (Sanderson & Booth, 1991).

Fractional Brownian motion can only yield a valid description of ocean surface drift trajectories over a finite range of space and time scales. This is because the relevant scales of turbulence are bounded above by the length of the drifter track (larger scales are filtered out as mean motion) and below by the small scales where one expects the dispersion to scale as t^2 (Taylor, 1921). The range of spatial scales over which fBm may be applied is generally thought to correspond with the range over which a drifter trajectory exhibits fractal characteristics (Osborne et al., 1989; Sanderson & Booth, 1991). This range can be determined using the "yardstick" method (cf. Osborne et al., 1989; Thomson & Emery, 2014), where the length of the trajectory L is measured as a function of the length of the "ruler" (or yardstick) with which it is measured, denoted as Δ. If the trajectory exhibits fractal characteristics the length L will scale logarithmically with yardstick length as

$$L(\Delta) \propto \Delta^{1-D} \tag{5}$$

where D is the fractal dimension (also refered to as the "divider dimension" D_L in the literature). Therefore, the range of scales over which the trajectory has fractal characteristics can be determined by plotting $L(\Delta)$ versus Δ in log-log space and determining whether L evolves linearly over any particular domain of Δ. If such a domain exists, the slope is $1 - D$.

Spectral methods for analyzing fBm are less well-defined. The spectral properties of the position statistics of fBm, which are nonstationary, are not easily defined using traditional Fourier transforms and are not considered in detail in this paper. However, it is generally accepted that the power spectrum of drifter positions with fractal dimension D is proportional to $f^{-(2/D+1)}$ (Osborne et al., 1989; Sanderson & Booth, 1991). This relationship might therefore be used to provide an additional estimate of fractal dimension if the power spectrum of drifter displacements is known. For example, if $D = 1.3$ we expect a position variance spectrum $\propto f^{-2.5}$. However Osborne et al. (1989) note that spectral slope alone cannot be considered indicative of fractal behavior. This must be confirmed by the yardstick method or other equivalent techniques. Readers

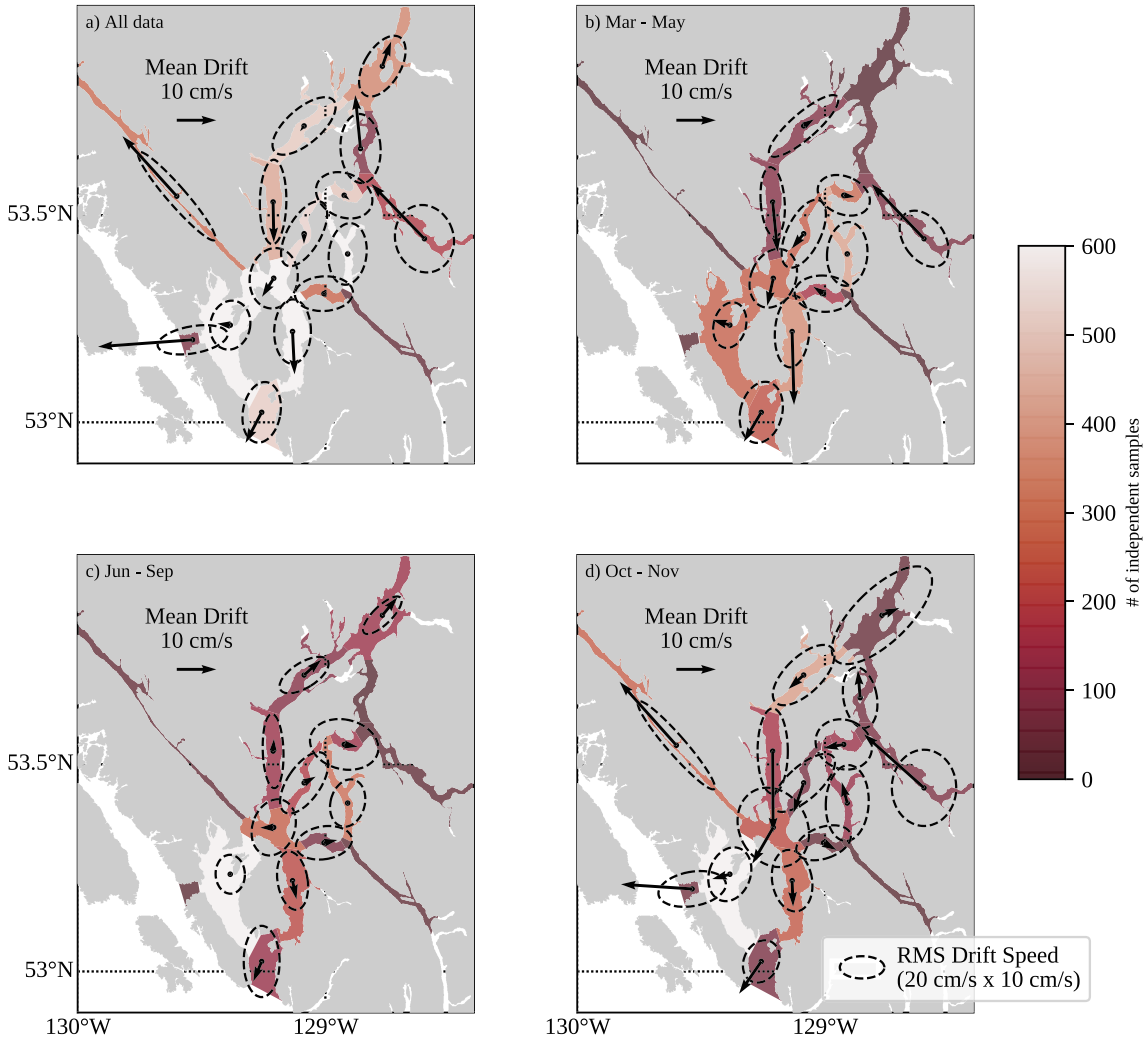

Figure 4. Distribution of mean (arrows) and RMS (dashed ellipses) drift velocities in the Kitimat system. Results are shown of the average over the data set (a) along with seasonal averages (b–d). Shading indicates the number of independent samples of drift velocity in the regions over which statistics were derived.

interested in the relationship between fractals and spectral analysis may refer to Lilly et al. (2017) and the references therein for a more detailed discussion.

4. Results

We now begin our analysis of the data described in section 2, using the methods outlined in section 3.

4.1. Mean Drift Patterns and Driving Forces

Ocean surface drift in the Kitimat fjord system exhibits significant seasonal variability, but is generally directed seaward as is expected in an estuarine system (Figure 4a). Mean drift speeds generally range from 5–10 cm s^{-1} though they may reach magnitudes up to 24 cm s^{-1}. In the spring and fall mean drift is directed seaward everywhere except a few channels north of Wright Sound. In the summertime mean drift reverses direction everywhere north of Wright Sound and slows south of Wright Sound (Figures 4b–4d). The mean and largest RMS fluctuations of the drift velocities are well aligned with the main axis of the channels, however appreciable fluctuating cross-channel drift is also evident. Along-channel RMS fluctuations of velocity range from 22–52 cm s^{-1}, while cross-channel fluctuations range between 8 and 26 cm s^{-1}.

The mean and RMS drift patterns shown in Figure 4 are quite different from similar maps of near-surface currents (7–10 m depth) (Figure 2). Mean surface drift velocities regularly exceed mean currents by a factor of 2 or more, and sometimes mean drift is directed opposite to recorded mean near-surface currents. RMS

drift velocities are also larger than RMS currents, both in the along-channel and cross-channel directions. This suggests that currents in the upper ~10 m of the water column are strongly sheared, which could be attributed to strong stratification, wave-induced currents, and some wind-induced slippage of the drifters.

Near-surface velocity shear can be quantified by a single-parameter regression analysis comparing along-channel drift velocity u_{drift_X} near mooring FOC1 to currents recorded at 7–10 m depth (u_{current_X}) and winds recorded 5 m above the water surface at Nanakwa Shoal (u_{wind_X}) (see Figure 1). Fitting all available drifter data to a linear model of the form $u_{\mathrm{drift}_X} = \alpha u_{\mathrm{wind}_X} + u_{\mathrm{current}_X}$ explains 50% of the variance in the along-channel drift with a regression coefficient $\alpha = 0.042$. The coefficient varies seasonally, from 0.024 in summer to 0.048 (0.05) in spring (fall). These values are similar to those found by Wan et al. (2017), who investigated the relationship between winds and currents at 4–7 m depth for a subset of the time period considered here. Similar to their results, we find that our regression model has more explanatory power in spring/fall ($r^2 = 0.58/r^2 = 0.43$) than in summer ($r^2 = 0.34$) (Table S1 and Figure S7). Regression using information on both wind and currents yields a better description than using only currents ($r^2 = 0.34$) or only winds ($r^2 = 0.32$). Therefore, knowledge of both currents and winds is required for drift prediction. Note that the results discussed here are limited to wind speeds below 7 m s^{-1}, as there were no drifter observations coinciding with higher wind speeds.

4.2. Along-Channel Drift and Dispersion

The along-channel drift and dispersion of all drifters in the data set can be visualized as the distribution of displacements as a function of time scale (Figure 5). The displacements are one-dimensionalized as described in section 3.1, and taken as positive toward the ocean and negative toward land. The distributions indicate a seasonally varying mean seaward drift, consistent with section 4.1, and very rapid dispersion within the first 24 hr, as indicated by the increase in the width of the distribution. Dispersion begins to slow noticeably after 24 hr and displacements become increasingly uniformly distributed with time.

The mean seaward drift ranges from 1.4–7.5 cm s^{-1} through the seasons, with a mean value of 4.4 cm s^{-1} (Figure 5). It is strongest in the fall and spring and insignificant (<2 cm s^{-1}) in the summer. This is consistent with the previous observation that up-channel winds can effectively stop, or even reverse, the estuarine outflow at the very surface of the water column in Douglas Channel (Wan et al., 2017). In region SOUTH (south of Wright Sound) mean seaward drift is twice as fast as in regions DC (Douglas Channel) and EAST (east of Douglas Channel) (Figure 5). The mean drift appears to be constant, as evidenced by the good linear regression fit to the time-evolving mean displacement values, except when considering the regional subsets DC and EAST (Figure 6). The exception is likely due to an increasing number of drifters entering the less energetic regions near the shoreline in these smaller channels, while some fast-moving drifters closer to the channel centreline exit the region more quickly. The calculated mean displacement at longer times would therefore be biased toward slow-moving drifters. This is evidenced in the increasingly 'deterministic' character of the displacement distributions for these subregions, where trajectories of individual drifters are clearly visible at longer times (Figures 5e and 5f).

Dispersion of the drifters about the mean (indicated by the width of the distributions of ΔX in Figure 5) suggests that drifters may disperse over the length of the Kitimat fjord system (~140 km) over a period of 7 days. The dispersion is stronger in the fall than in the spring, and weakest in the summer (Figure 5), similar to trends in the mean drift. Dispersion is also stronger in the region SOUTH than in the regions DC and EAST. This may also be due to the relatively larger area covered by SOUTH and the resulting bias toward slow-moving drifters at longer times in DC and EAST.

The displacement variance (or dispersion) evolves with rapid initial growth (the ballistic regime) which slows at longer times (the diffusive regime). This is consistent with previous studies of drifter dispersion in the open ocean (cf. Poulain & Niiler, 1989) and the dispersion theory of Taylor (1921). We fit power laws of the form At^B, where A and B are free parameters, to the observed time-evolving displacement variance and delineate the time of transition between the ballistic and diffusive regimes, t_T, as the time which minimizes the overall error in the regression fit (Figure 6). In the ballistic regime variance grows according to $\sigma^2 \propto t^{1.5}$, which slows to $\sigma^2 \propto t^{0.85}$ in the diffusive regime. A transition time of 15 hours yields the best regression fits for the complete data set. There is some variation in these values among seasonal and regional subsets of the data (see Table 1). The 95% confidence intervals of a Gaussian distribution calculated using the time-evolving mean and variance from Table 1 are a good match to the range within which 95% of the drifters are observed (Figure 5).

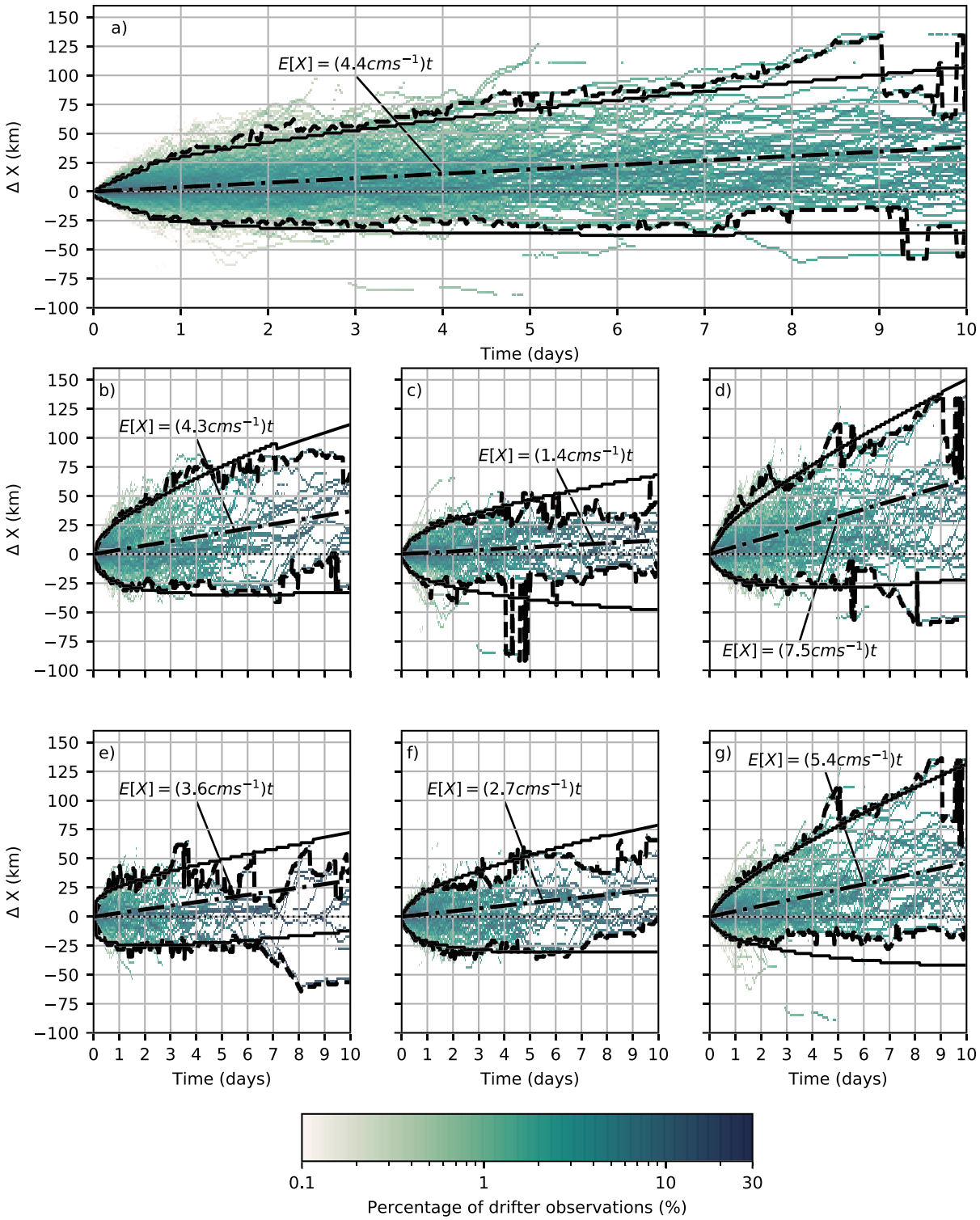

Figure 5. Distribution of drifter displacements, ΔX, over 10 days with mean (dash-dotted line, with implied mean drift speed), 95% limits (dashed line), and 95% limits of the corresponding normal distribution (solid line). Distributions are derived by binning observed displacements into 2 km by 0.5 hr bins, and for each half hour interval reporting the percentage of observed displacements in each displacement bin. Results are shown for the complete data set (a), as well as seasonal subsets of data from March to May (b), June to September (c), and October to November (d), and regional subsets for DC (e), EAST (f), and SOUTH (g).

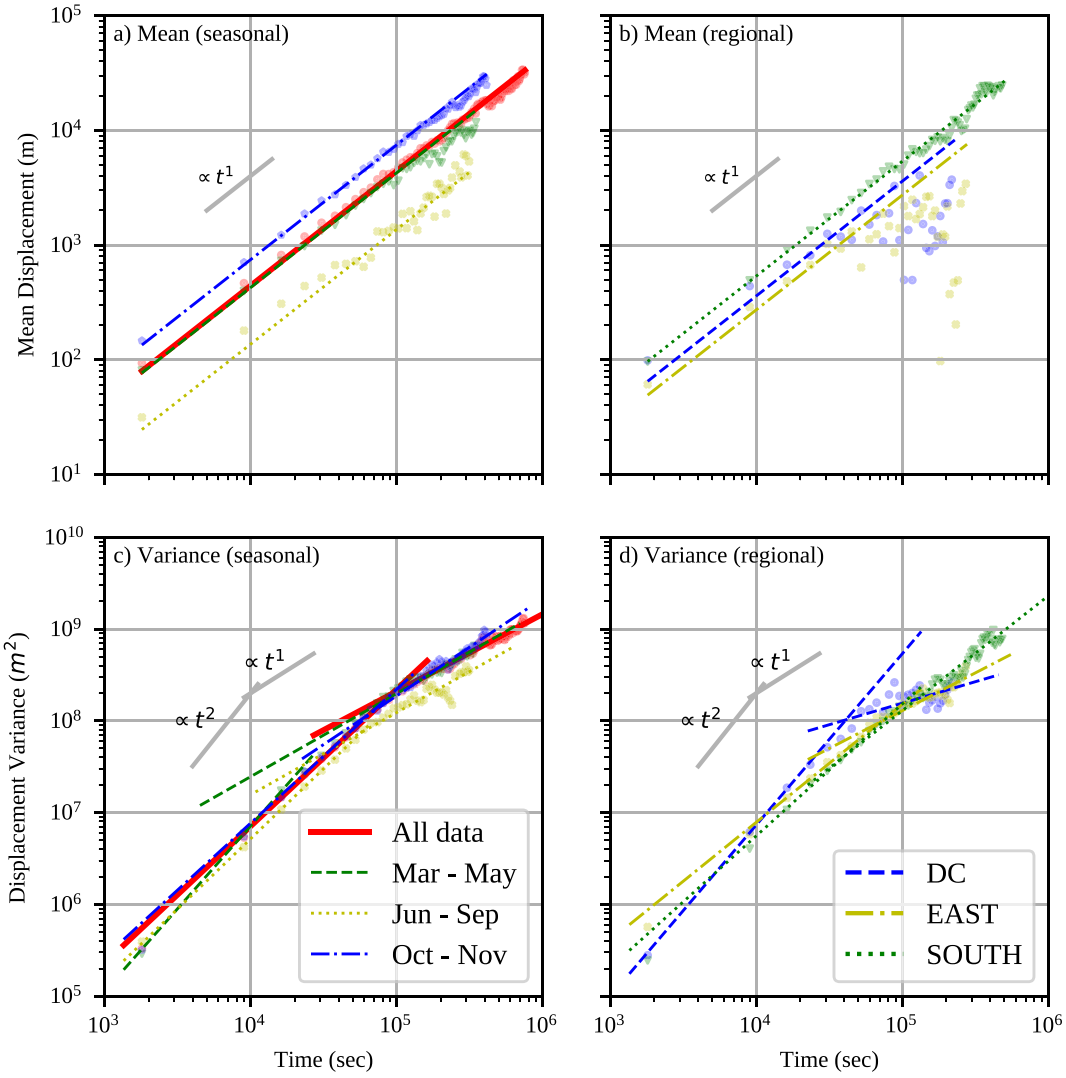

Figure 6. Mean and variance of drifter displacement, ΔX, as functions of time for the seasonally resolved (a, c) and regionally resolved (b, d) data. Optimal linear (power-law) regression fits are superimposed on the plotted mean (variance). Fit parameters are given in Table 1.

The skewness and kurtosis of the displacement distributions indicate that up-channel displacements are more frequent while down-channel displacements are larger in the sense of extremes (consistent positive skewness), and that for times <3 days extreme displacements are more likely than a normal distribution would predict, that is, the distributions are leptokurtic (kurtosis > 3) (Figure S8).

4.3. Effects of Cross-Channel Dispersion

Over the course of the experiments it was noted that drifters tended to ground ashore quite frequently, despite being released near midchannel. To quantify this tendency, we examine the distribution of normalized proximity to the shoresline, χ. This indicates that on average a drifter will move from midchannel ($\chi > 0.8$) to near the shoreline ($\chi < 0.1$) within 13.5 hr (Figure 7a). The frequency distribution has the character of an extreme value distribution, with short times being more frequently observed (Median = 9.9 hr, Mode = 5.3 hr), though some drifters remain near midchannel for more than 48 hr. The statistics of χ are relatively consistent seasonally (Figure S9).

Nearshore drift velocity statistics differ appreciably from velocity statistics near midchannel. For example, in upper Douglas Channel mean and RMS along-channel velocities near the shore are approximately half of those in midchannel. Kurtosis increases near the shore even though extreme values are comparable, indicating that slow drift velocities occur more frequently in the nearshore. Cross-channel velocities remain

Table 1
Regression Fit Parameters Describing the Evolution of the First Two Moments of Observed Displacement Probabilities

Season	Region	Mean (cm s^{-1})	A_b	B_b	A_d ($\times 10^3$)	B_d	τ_T (hr)
All	System	4.42 ± 0.02	7.7 ± 0.91	1.49 ± 0.01	12.9 ± 1.86	0.84 ± 0.01	15.0
Spring		4.26 ± 0.02	0.44 ± 0.15	1.80 ± 0.04	5.88 ± 0.91	0.90 ± 0.04	2.5
Summer	System	1.37 ± 0.04	3.98 ± 1.73	1.53 ± 0.04	4.11 ± 2.12	0.90 ± 0.04	6.0
Fall		7.46 ± 0.03	11.3 ± 2.7	1.46 ± 0.02	0.931 ± 0.261	1.06 ± 0.02	12.5
	Douglas	3.60 ± 0.07	0.25 ± 0.04	1.87 ± 0.02	710 ± 396	0.47 ± 0.05	2.0
All	Eastern	2.73 ± 0.11	57.2 ± 22.1	1.28 ± 0.04	9.94 ± 4.72	0.82 ± 0.04	12.0
	Southern	5.37 ± 0.05	9.98 ± 2.79	1.44 ± 0.03	0.0715 ± 0.0360	1.25 ± 0.04	15.0

Note. Linear fits describe the mean, and power laws of the form $\sigma^2 = A\tau^B$ describe the two regimes of variance growth (ballistic, subscript b, and diffusive, subscript d). τ_T is the time of transition between the regimes, determined as the time which minimizes the total error in the regression fits to the observed variance.

much more consistent than along-channel velocities (Figures 7b and 7c). Averaging results from all drifters supports the notion that mean drift speed in midchannel is approximately twice as large as speeds near the shoreline (Figure S10). Therefore, the significant decrease in along-channel dispersion after ~15 hr observed in section 4.2 can be explained by majority of drifters' tendency to move into less-energetic nearshore regions within that time.

4.4. Spectra and Fractal Dimension

To further characterize the dynamics of the drifter motion, we estimate the energy spectrum $P_e = 0.5(P_{uu} + P_{vv})$ of drift velocity. Here P_{uu} and P_{vv} are the power spectra of drift velocity in the east-west and north-south directions, derived using Welch's average periodogram method. Global coordinates are used here since the energy spectrum is invariant under coordinate rotations. Time series are separated into segments consisting of 512 data points at 15 min intervals (128 hr), with 50% overlap, and a Hanning window is applied to reduce leakage. Only time series longer than 24 hr are considered, and they are zero-padded where required.

P_e indicates appreciable influence of the semidiurnal tide and decreasing energy toward higher frequencies, with the mean spectrum scaling as $\propto f^{-1.9\pm1.69}$ at frequencies higher than 0.1 cycles per hour (cph) (top panel of Figure 8). The uncertainty estimate on the spectral slope indicates 1 standard deviation. At the M2 frequency a widened peak is evident in the spectrum, but no peak is evident at the diurnal (K1) frequency. This may be due to the fact that the majority of the drifters come in close proximity of the shoreline within less than 24 hr, which exposes them to a velocity field that differs from midchannel. Summertime drifter

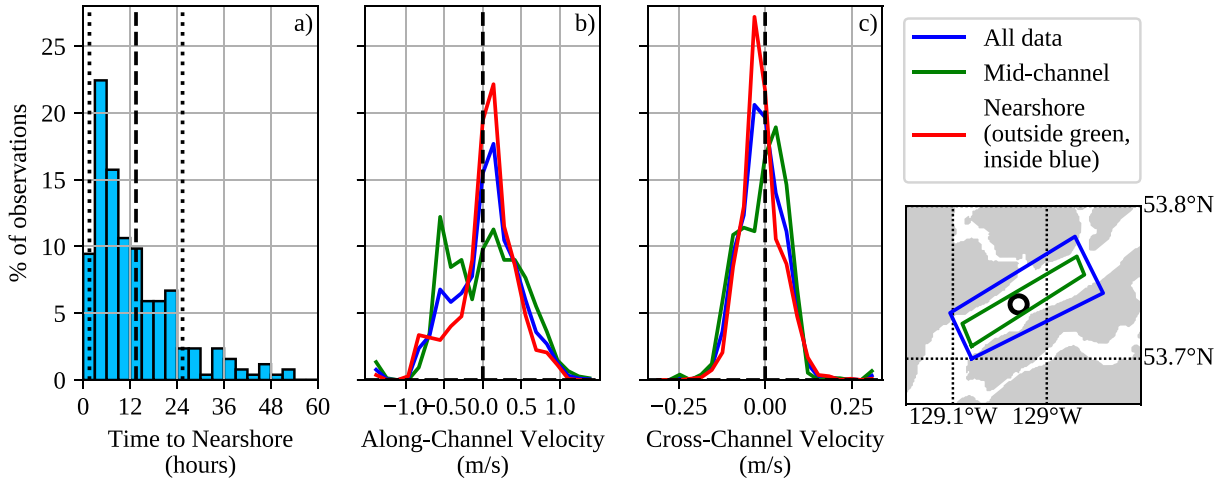

Figure 7. (a) Distribution of times taken for a drifter to move from midchannel ($\chi > 0.8$) to near the shoreline ($\chi < 0.1$). Mean time is indicated by the dashed black line and dotted lines indicate one standard deviation around the mean. (b,c) Distributions of drifter along- and cross-channel velocities near midchannel (shown in green; inside green polygon), near the shore (shown in red; inside blue polygon, outside green polygon), and for all data (shown in blue; inside blue polygon). Along-channel velocity is positive down-channel (approximately southwest) and cross-channel velocity is positive 90° clockwise from down-channel (approximately northwest).

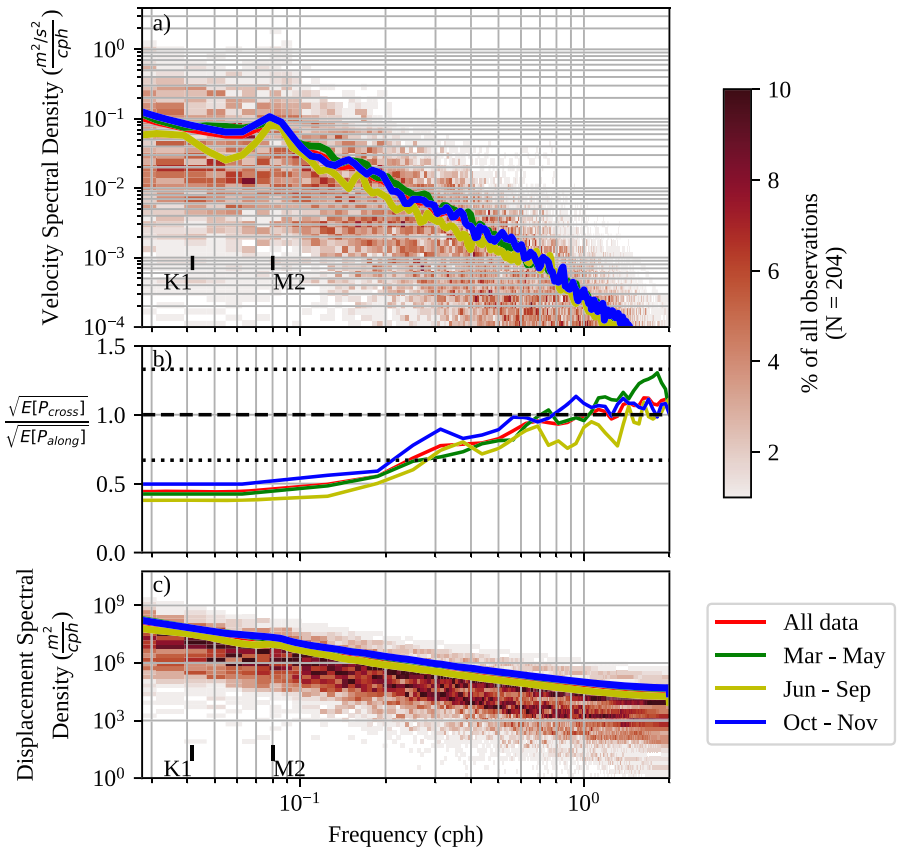

Figure 8. (a) Mean energy spectra of drift velocity $0.5(P_{uu}+P_{vv})$ for the complete data set (red), as well as spring (green), summer (yellow), and fall (blue). Binned density of observations from individual drifter tracks are shown by the colorbar. (b) Ratio of mean amplitude spectra of velocity in the cross-channel: along-channel directions as a function of frequency for all data (red), spring (green), summer (yellow), and fall (blue). Bounds for approximately isotropic motion are indicated by the dashed lines. (c) Energy spectrum of drifter displacement in the same style as (a).

motion is less energetic than motion in the spring and fall. As a result, the semidiurnal tidal peak is more pronounced, and the overall lower energy level at low frequencies suggests lessened dispersion on longer time scales (LaCasce, 2008), which is consistent with Figure 5.

For later comparison with the theory of fractional Brownian motion, we note that corresponding energy spectra of displacement (bottom panel of Figure 8) scale between $f^{-2.23\pm0.46}$ (spring) and $f^{-2.47\pm0.66}$ (summer) with an average of $f^{-2.31\pm0.53}$.

The ratio of cross-channel: along-channel velocity amplitude spectra suggests that within the channels drifter motion is isotropic on time scales shorter than 3.5–5 hr to within $\sqrt{E[P_{\text{cross}}]}/\sqrt{E[P_{\text{along}}]} = 1 \pm 0.3$, following Sanderson and Booth (1991)'s argument for isotropy (middle panel of Figure 8). Repeating this calculation in global u,v coordinates suggests isotropic motion on time scales up to 10 hr (Figure S11). We therefore conclude that drifter motion is sufficiently isotropic to potentially be described by fractional Brownian motion on time scales up to at least 3.5 hr, and up to 10 hr in areas where the distinction between along-channel and cross-channel direction is not clear (e.g., in Wright Sound or Squally Channel). On longer time scales along-channel motion becomes significantly more energetic as cross-channel motion is limited by drifters reaching nearshore areas.

The drifters display fractal behavior with a dimension, D, of 1.34 over scales ranging from 2–13 km, which corresponds well to the width of the channels in the Kitimat fjord system (Figure 9). The fractal dimension of the shoreline over these scales ($D = 1.26$), estimated using the yardstick method and coastline data from the GSHHS database (Wessel & Smith, 1996), is similar to the value reported for the west coast of Britain (one of the "most irregular in the world," with $D = 1.25$) (Mandelbrot, 1967). The fractal dimension of the shoreline is less than that of the tracks, which range from $D = 1.31$ (1.30) in the spring (fall) to $D = 1.46$ in

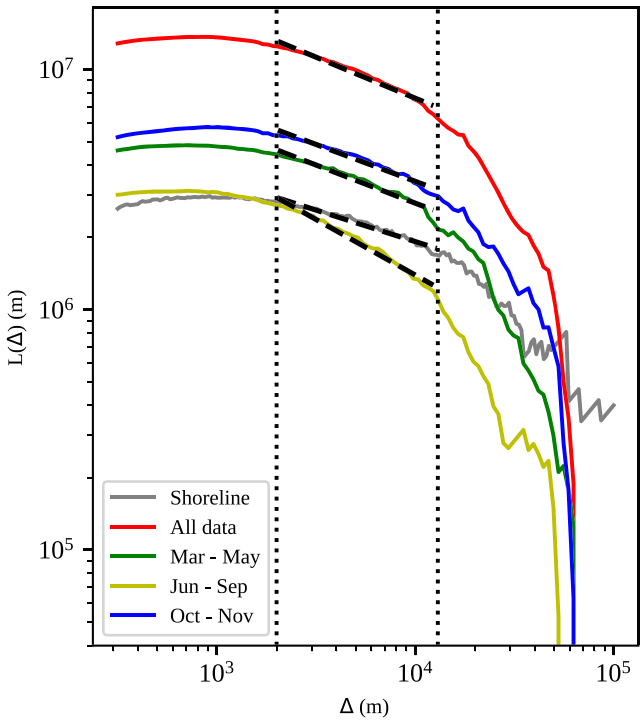

Figure 9. Yardstick trajectory length estimates for shoreline, and drifter tracks with seasonal subsets. Dashed lines show log-transformed regression fits to $L(\Delta)$, with slopes $1 - D_L$. Regression results are reported in Table 2. Dotted vertical lines indicate the range of spatial scales over which fractal behavior is evident.

the summer (Table 2). This indicates that drifters are occupying space both parallel to and orthogonal to the coastline and that more cross-channel, space-filling motion occurs in summer than in spring and fall.

5. Discussion

The above results suggest that in general drifters in the Kitimat fjord system disperse isotropically for up to 10 hr after deployment while being moved seaward by the mean flow. Drifters that come very close to the shoreline slow down and thereby slow the along-channel dispersion. Along-channel dispersion continues in a slowed manner and together with constant mean seaward transport results in drifters being dispersed over scales up to the size of the Kitimat fjord system within 7 days. These dynamics are driven by a combination of tidal currents, density-driven estuarine flow (resulting in mean seaward motion), and wind-induced circulation. None of these processes are negligible for drift prediction, and information on both currents and winds is required to optimally characterize surface drift.

Table 2
Fractal Dimensions Derived from Log-Transformed Regression Fits in Figure 9 ($D = 1 - slope$), Power Law Exponents ($\sigma^2 \propto t^B$) Predicted by Fractional Brownian Motion ($B_{predicted}$), and Those Observed During the First 15 hr of Dispersion-Based Regression Fit to Observations of Displacement Variance Growth ($B_{observed}$)

Case	D	$B_{\text{predicted}}$	B_{observed}
Shoreline	1.26 ± 0.01	-	-
All Data	1.34 ± 0.01	1.49 ± 0.01	1.49 ± 0.01
Spring	1.31 ± 0.01	1.53 ± 0.01	1.54 ± 0.02
Summer	1.46 ± 0.01	1.37 ± 0.01	1.48 ± 0.03
Fall	1.30 ± 0.01	1.54 ± 0.01	1.44 ± 0.02

The assumption that the statistics of drifter displacement are stationary is considered tenable, and necessary to the analysis, while acknowledging that the differences between summer and spring/fall, and regions SOUTH and DC/EAST, imply some nonstationarity in the total data set. The mean and variance of ΔX remain on the same order of magnitude for all subsets of the data. Also, the differences between the higher moments for subsets of the data is generally less than the variability of these moments, that is, the standard deviation of an individual time series of skewness/kurtosis, over 10 days. We do not consider the seasonal and regional variability of the statistics to be significant enough to void the assumption of stationary statistics.

The power laws describing the evolution of the drifters' displacement variance exhibit some similarities to previous descriptions of single-particle dispersion. The two-regime structure of variance growth agrees with the theory of Taylor (1921), though the power law exponents are less than those proposed by this theory. Taylor (1921) proposes $\sigma^2 \propto t^2$ in the ballistic regime and $\sigma^2 \propto t^1$ in the diffusive regime, whereas we find $\sigma^2 \propto t^{1.5}$ (ballistic) and $\sigma^2 \propto t^{0.84}$ (diffusive). This is hardly surprising, as the theory explicitly assumes homogeneous, isotropic turbulence which does not appear to be applicable across the width of the channels, though we do not preclude the possibility that $\propto t^2$ dispersion holds at very small time and space scales. However, anomalous (non-Taylorian) dispersion can occur in systems where long-term autocorrelations exist in the flow, or the flow is strongly affected by boundaries (Artale et al., 1997).

Fractional Brownian motion (section 3.3) may provide a suitable model for isotropic single-particle dispersion in the ballistic regime since the drifter trajectories exhibit fractal properties over spatial scales ranging from 2 to 13 km. Turbulent motion over time scales less than ~3.5–10 hr is also reasonably isotropic. Therefore the fractal dimension D can be used to estimate the power law for variance growth as $\propto t^{1.49}$, according to equation (4) (Sanderson & Booth, 1991). This matches the value observed over time lags of up to 15 hr. For seasonal subsets of the data the observed exponents are within 10% of those predicted by fractional Brownian motion when power laws are fitted to variance in the first 15 hr (Table 2). Note that these exponents may not be consistent with those presented in Table 1, which were derived by optimizing the regression fit through varying the time of transition between the ballistic and diffusive regimes. Given the good agreement of observed and modeled rates, we suggest that dispersion may be reasonably well modeled as isotropic fractional Brownian motion for up to 10 hr after release. In fact, solving for the time required for dispersion across a 5 km wide channel by assuming that the ballistic power law for along-channel dispersion from Table 1 applies and solving $\sigma^2 = \pi(2,\ 500\ \ \mathrm{m})^2 = 7.7t^{1.49}$ results in $t = 5.5$ hr, which corresponds well with the most frequently observed time required for a drifter to reach nearshore areas (the mode of distribution shown in Figure 7a). Leptokurtic displacement distributions, as were described in section 4.2, are also consistent with fractional Brownian motion. Similar to Sanderson and Booth (1991), we observe excess kurtosis that is even greater than the theoretically predicted value.

The mean slopes of the displacement energy spectra of drifter motion, s (Figure 8) suggest fractal dimensions ranging from 1.36 (summer) to 1.63 (spring) with a mean value of 1.53. These values differ from those calculated using the yardstick method described in section 3.3, and the difference is 2 times larger than the variability between fractal dimensions estimated for the same data by various methods reported by Osborne et al. (1989). Some variability between methods is expected, and the increased variability may in part be due to the fact that Osborne et al. (1989) considered mesoscale turbulence while we are concerned with submesoscale, confined motions above the tidal frequencies which are more susceptible to deterministic perturbations like the influence of local topography. We also note that the relatively large standard deviation of measured spectral slopes implies that the entire parameter space $1 \leq D \leq 2$ is contained within the standard deviation of the spectral slope estimate for summertime data. In spring and fall the parameter space is only slightly more constrained, covering $1.16 \leq D \leq 2$. We therefore conclude that while the measured displacement spectra are not in disagreement with fBm, they also do not offer information that could be used to usefully constrain the parameters of fBm. Hence, it is possible that fBm does not provide a valid theory for modeling drifter dispersion in some areas of the Kitimat fjord system at some times. However, given the evidence presented earlier we consider fBm with a fractal dimension of $D \approx 1.2$–1.6 to provide a credible estimate of isotropic drifter dispersion on time scales up to 3.5–10 hr and spatial scales from 2 to 13 km.

Proper characterization of cross-channel dispersion is especially important, as cross-channel motion has a significant impact on the overall transport behavior of the drifters. We claim that the transition of along-channel dispersion from the ballistic to the diffusive regime is likely driven by cross-channel dispersion of drifters into less energetic nearshore areas, citing the strong correspondence between the transition

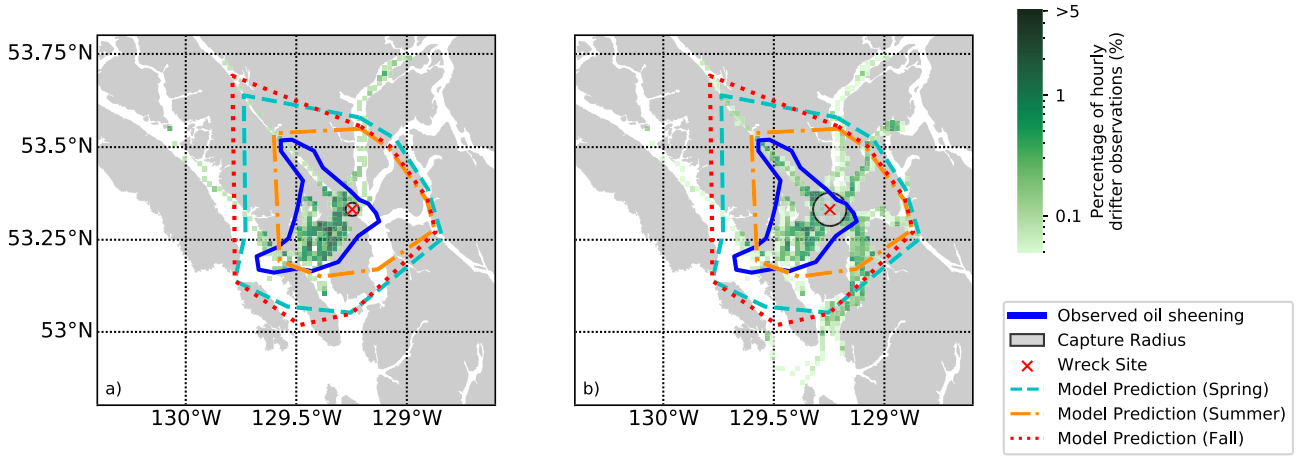

Figure 10. Density of hourly drifter positional fixes up to 48 hr after passing within 2 km (a) and 5 km (b) of the site of the wreck of the *Queen of the North*. Observations of oil sheening resulting from the wreck after 48 hr are shown in blue. Potential seasonal maximum spill extents predicted by applying a normal distribution with mean and variance specified by the regression fits from Figure 6 are shown in cyan (spring), orange (summer) and red (fall).

timing and the mean transport time from midchannel to the nearshore as evidence. This cross-channel dispersion is likely driven by a number of processes, such as (1) nonrectilinear tidal ellipses and corresponding cross-channel tidal excursions, though these are generally small (~500 m); (2) topographically driven eddies, which are likely to occur frequently in the Kitimat fjord system considering the appreciable roughness of the coastline; (3) shear dispersion generated by increased wind-driven currents near the centerline of the channel; (4) cross-channel transport of drifters with winds that are not perfectly aligned with the channel axis.

Internal wave activity (as previously reported on by ; Webster, 1983) may also contribute to cross-channel shear dispersion. Analysis of CTD profiles shows that on average internal Mode 2 (and higher) exhibit Rossby radii, R_i, less than or equal to the channel width, W, (4–6 km for Mode 2, 2.5–3.5 km for Mode 3) with strong surface intensification (Figure S12). This suggests that rotational dynamics may be important but not dominant, as the channels fall into an intermediate regime where $W/2 < R_i < W$ (Valle-Levinson, 2008; Rabe & Hindson, 2017). More work is needed to fully understand the dynamics governing cross-channel dispersion of drifters in the Kitimat fjord system, but this is beyond the scope of this paper and will be addressed in future work.

6. Application to Oil Spill Risk Analysis

The results presented in section 4.2 form a useful basis for predictions about the absolute dispersion of drifters in the along-channel direction. This could have important implications for assessing potential oil spill trajectories in the Kitimat fjord system.

The dynamical response of surface drifters varies considerably with draft, and therefore the behavior of a drifter must be experimentally compared to that of an oil spill before drifter observations can be used as a proxy for spilled oil. In 2006, the passenger ferry *Queen of the North* sank near the mouth of Douglas Channel. This incident resulted in a spill of ~220,000 L of diesel fuel and tragically claimed the lives of two passengers. To assess the similarities between spilled oil and the drifters considered here, we compare drifter tracks passing the incident site to observations of oil sheening within 48 hr of the incident (Harper et al., 2007). The cumulative density of positional fixes collected by drifters within 48 hr after passing within 2 and 5 km of the incident site is shown in Figure 10. Tracks passing within 1 and 10 km were also compared, but were not significantly different from the 2 and 5 km cases (not shown).

This comparison suggests that the observed drift may be an adequate proxy for the transport of spilled oil. For the 2 km case (left panel of Figure 10), the agreement between the drifter tracks and the observations of the diesel sheen is very good. Within 48 hr of passing the wreck site, 88% of the hourly drifter positions are recorded within the area where oil sheening was observed, and the drifters cover 80% of this area during that time. The majority of areas where drifters exited the region of observed oil sheening are areas where

appreciable uncertainty in the sheening observations is noted (Harper et al., 2007). Also, given seasonal and interannual variability in the circulation, it is not surprising that some drifters traveled outside of the area where the diesel slick was observed. We note however that no drifters passing within 2 km of the incident site traveled into the channels connecting to Wright Sound from the east. This differs for the 5 km case (right panel of Figure 10), as the majority of drifters passing within 2–5 km of the wreck site occupy the channels connecting to Wright Sound from the east. The number of available drifter tracks approximately doubles for this case, however the percentage of fixes in the area with reported sheening drops to 57%. This suggests that trajectories of surface drifters and oil spills from Wright Sound are highly sensitive to initial location. Local residents' observations of diesel sheen in Whale and Ursula Channel in the year following the incident support the notion that transport of oil from Wright Sound to these regions is possible (Harper et al., 2007).

As the drifters appear to be a reasonable proxy for spilled oil, we can use the results from section 4.2 to model the possible extents over which oil may be transported, noting a few cautions and assumptions. By taking only the along-channel dispersion into consideration, we assume that oil spreads across the channel quickly. This is supported by the rapid cross-channel motion noted in section 4.3, and we note that gravitational spreading of a large oil spill would speed cross-channel dispersion up further. We also caution readers that taking the drifters described here to be a suitable proxy for spilled oil is likely not a universal result, since the behavior of different oil slicks may vary appreciably depending on the physical and chemical properties of the slick. Also, the modeling approach proposed here should only be applied for times between the months of March and November. No drifter data is available to inform the choice of model parameters outside of these months, and the effect of changes in wind patterns and stratification on surface drift is not readily estimated without additional data collection or verifiable numerical modeling.

Acknowledging these caveats, equation (2) can be used to model the area within which we would expect to find 95% of the oil spilled from the wreck of the *Queen of the North* within the first 48 hr. We calculate $\mu(\tau)$ and $\sigma^2(\tau)$ using values from Table 1. The parameter $\mu(\tau)$ is the product of the mean drift (third column) and $\tau = 48$ hr, and $\sigma^2(\tau) = A_d \tau^{B_d}$. We use the diffusive parameters to calculate $\sigma^2(\tau)$, as 48 hr is outside of the ballistic regime and predict that the maximum drifter (or oil) displacement will be 27–32 km upstream of the initial location and 28–50 km downstream, with exact values depending on season (Figure 10). The area described by these displacements from the wreck site fully encompasses the area within which oil sheening was observed after the incident, and they are a good match with observed drifter positions within 48 hr of passing within 5 km of the wreck site of the *Queen of the North*.

The area where oil is predicted to be found is larger than the reported oil sheen observation, which can be expected for two reasons. First, by applying equation (2) in the manner presented in Figure 10 we assign each channel equal likelihood of drifters (or oil) entering it, as we cannot statistically resolve the dispersion between the channels. This is a major assumption which is supported by the fact that our predictions are in much better agreement with the drifters passing within 5 km of the wreck site than with those passing within 2 km. Since trajectories are sensitive to initial position, and the location of an oil spill is often not known precisely in operational scenarios, we suggest that assuming equal likelihood or oil presence in each channel is appropriate. The second reason we expect the predicted area to be larger than the area of observed oil sheening is that the sheening is only one realization of a stochastic process (dispersion from the wreck site), while the prediction refers to the 95% confidence intervals of this process. Each drifter (or group of drifters) passing the wreck site is an independent realization of the process, however, and consequently, the footprint of the drifter data is larger than the observed sheened area. In the spring and fall, 91% of the observed drifter data was recorded within the area predicted by the model, though that number falls to 80% in the summer. These values are only slightly smaller than the expected 95%, and the misfit can be attributed to the excess kurtosis of the displacement distributions.

As an alternative to using observationally derived parameters in equation (2), dispersion may be modeled using generalized results from previous work. This approach is attractive as it does not require additional data collection. To the best of our knowledge Okubo (1971) is the best available source of general dispersion estimates for this application; however, some differences between his work and that presented here must be considered. Okubo (1971) measures dispersion as dye patch size, whereas we consider single-particle statistics. Therefore, the apparent diffusivity, K_a, at large scales appears to be the reasonable metric for comparison since we expect that K_a from multiparticle statistics converges to K_a derived from single-particle statistics as the patch size and dispersion time approach the decorrelation scales of the velocity field. Our

results suggest $K_a = \frac{1}{2}\frac{d\sigma^2(\tau)}{d\tau} = \frac{1}{2}A_d B_d \tau^{B_d - 1} = 7.9 \times 10^6$ cm^2 s^{-1} at $\tau = 48$ hr (with A_d and B_d from Table 1, in units of meters and seconds, respectively). This is near the upper limit of the range of apparent diffusivities at spatial scales of ~100 km presented in Figure 4 of Okubo (1971) and larger than the diffusivity implied by regression fit to their data.

There are several reasons we expect our data to imply slightly higher diffusivity than the results of Okubo (1971). The first is that 48 hr may not be enough time for estimates of K_a from multiparticle and single-particle statistics to converge. Also, the along-channel axis is clearly the major axis of dispersion (see Figures 4 and 7) and therefore applying dispersion along this axis isotropically will result in a larger estimate of diffusivity than Okubo (1971), who distinguishes between major and minor axis dispersion. Finally, we note that Okubo's (1971) data points for diffusivity at scales larger than 10 km are predominantly from experiments in the North Sea, and currents and turbulence levels during these experiments were likely less than in the Kitimat fjord system where currents and turbulence are amplified by topographic restrictions on the flow.

We propose that single-particle statistics are appropriate for our application, as the purpose of our model based on equation (2) is to predict the farthest extents that oil may have drifted to, rather than the change in size of an oil slick due to dispersion of the oil. Since the relationships proposed by Okubo (1971) cannot be used to successfully recover the associated diffusivity, we conclude that dispersion parameters for the Kitimat fjord system and dynamically similar regions should be derived from observations, as was done here, until sufficient data are available to expand the work of Okubo (1971) to include multiply connected fjord systems.

The effect of mean drift should also be considered. We note above that our predictions are better in the spring/fall than in the summer, and since the mean drift is nearly negligible in the summer data, this suggests that including a mean drift improves predictions. Equation (2) allows for a mean drift, and it does not appear that this equation can easily be simplified further. Applying a constant mean and constant dispersion rate would simplify the mathematics; however, the observed rate of dispersion decreases with time due to drifters approaching the shoreline, and therefore a constant dispersion rate would result in overestimation. For these reasons we propose that modeling the possible extents of along-channel transport using equation (2) strikes a good balance between simplicity and accuracy.

7. Conclusions

We have investigated the mean drift and dispersion of 206 novel ocean surface drifters deployed in the Kitimat fjord system between 2014 and 2016. To the best of our knowledge this is the most extensive set of drifter data collected in a fjord system to date.

The drifters exhibit a mean seaward motion through the study region, which is consistent with previously described estuarine circulation patterns (Wan et al., 2017). Mean outflow is strongest in the spring and fall, which has been linked to strong up-channel winds occurring in the summertime. Along-channel dispersion of drifters is also strongest in the spring and fall, with some drifters dispersing over the length of the fjord system (~140 km) in 7 days. No drifter data is available during the winter months (beginning of December to mid-March).

On time scales longer than ~12 hr interaction with shorelines slows drifter dispersion to rates below those expected from the classical theory of Taylor (1921). The close match between the time required for drifters to reach less energetic nearshore regions and the timing of the slowing of along-channel dispersion suggests that rapid cross-channel dispersion is the root cause of slowed along-channel dispersion. On shorter time scales the observed dispersion is consistent with fractional Brownian motion (Sanderson & Booth, 1991), and the tracks are found to display fractal characteristics over scales of 2 to 13 km with fractal dimensions that are comparable to values from the literature.

The observed drift speeds are found to be best described by a combination of uppermost available currents in the water column and wind-driven term parameterizing near-surface current shear, wave-induced circulation, and some drifter slippage. Therefore, measurements of wind are needed to complement measurements of currents made with moored subsurface ADCPs to fully characterize the drift of objects at the ocean surface in the Kitimat fjord system. A seasonally resolved linear regression model for along-channel drift speed has been proposed.

Finally, the drifters are shown to be a reasonable proxy for oil sheening observed after an oil spill in the study region. A simple dispersion model based on the 95% confidence intervals of a Gaussian distribution fitted to the observed along-channel drifter displacements is found to well reproduce the area within which drifters or oil from a specified location can be found. This model may yield useful information for estimating the potential extent of oil transport after a spill in the Kitimat fjord system.

Acknowledgments
Hauke Blanken gratefully acknowledges financial support through the World Class Prevention, Preparedness and Response to Oil Spills from Ships Initiative, the Oceans Protection Plan, and a University of Victoria Graduate Student Fellowship. The manuscript was significantly improved by the suggestions of two anonymous reviewers, and we thank them for their thoughtful assessment of the work presented here. We would also like to thank Stephen Page for his assistance with collection and archiving of the drifter data, as well as the Captain, crew, and scientists aboard the *CCGS John P. Tully* and *CCGS Vector* for their assistance with data collection for this study. All data used in this study can be accessed at this site (www.waterproperties.ca).

References

Addison, P. S., Qu, B., Nisbet, A., & Pender, G. (1997). A non-Fickian, particle-tracking diffusion model based on fractional Brownian motion. *International Journal for Numerical Methods in Fluids*, *25*(12), 1373–1384.

Artale, V., Boffetta, G., Celani, A., Cencini, M., & Vulpiani, A. (1997). Dispersion of passive tracers in closed basins: Beyond the diffusion coefficient. *Physics of Fluids*, *9*(11), 3162–3171.

Breivik, Ø., & Allen, A. A. (2008). An operational search and rescue model for the Norwegian Sea and the North Sea. *Journal of Marine Systems*, *69*(1-2), 99–113.

Crawford, W. R., Cherniawsky, J. Y., & Cummins, P. (1999). Surface currents in British Columbia coastal waters: Comparison of observations and model predictions. *Atmosphere-Ocean*, *37*(3), 255–280.

Daniel, P., Jan, G., Cabioc'h, F., Landau, Y., & Loiseau, E. (2002). Drift modeling of cargo containers. *Spill Science & Technology Bulletin*, *7*(5–6), 279–288.

Davidson, F. J., Allen, A., Brassington, G. B., Breivik, Ø., Daniel, P., Kamachi, M., et al. (2009). Applications of GODAE ocean current forecasts to search and rescue and ship routing. *Oceanography*, *22*(3), 176–181.

Davis, R. E. (1985a). Drifter observations of coastal surface currents during CODE: The method and descriptive view. *Journal of Geophysical Research*, *90*(C3), 4741–4755.

Davis, R. E. (1985b). Drifter observations of coastal surface currents during CODE: The statistical and dynamical views. *Journal of Geophysical Research*, *90*(C3), 4576–4772.

Davis, R. (1987). Oceanic property transport, Lagrangian particle statistics, and their prediction. *Journal of Marine Research*, *41*, 163–194.

de Young, B., & Sanderson, B. (1995). The circulation and hydrography of Conception Bay, Newfoundland. *Atmosphere-Ocean*, *33*(1), 135–162.

Farmer, D. M., & Freeland, H. J. (1983). The physical oceanography of fjords. *Progress in Oceanography*, *12*(2), 147–219.

Fingas, M. (2011). Buoys and devices for oil spill tracking. *International Oil Spill Conference Proceedings*, *2011*, 213–228.

Freeland, H., Rhines, P., & Rossby, T. (1975). Statistical observations of the trajectories of neutrally buoyant floats in the North Atlantic. *Journal of Marine Research*, *33*, 383–404.

Guo, W., Wang, Y., Xie, M., & Cui, Y. (2009). Modeling oil spill trajectory in coastal waters based on fractional Brownian motion. *Marine Pollution Bulletin*, *58*(9), 1339–1346.

Hackett, B., Breivik, Ø., & Wettre, C. (2006). Forecasting the drift of objects and substances in the ocean. In E. P. Chassignet, & J. Verron (Eds.), *Ocean weather forecasting* pp. 507–523): Springer.

Harper, J., Bright, D., & Sanborn, M. (2007). *Queen of the north monitoring: Summary review*. Saanich, BC: Coastal & Ocean Resources Inc.

Huggett, W., & Wigen, S. (1983). Surface currents in the approaches to Kitimat. In R. W. Macdonald (Ed.), *Proceedings of a workshop on the Kitimat marine environment, Canadian technical report of hydrography and ocean sciences* (Vol. 18, pp. 34–65): Fisheries and Oceans Canada.

LaCasce, J. (2008). Statistics from Lagrangian observations. *Progress in Oceanography*, *77*, 1–29.

Lilly, J. M., Sykulski, A. M., Early, J. J., & Olhede, S. C. (2017). Fractional Brownian motion, the Matérn process, and stochastic modeling of turbulent dispersion. *Nonlinear Processes in Geophysics*, *24*(3), 481–514.

Macdonald, R., Bornhold, B., & Webster, I. (1983). The Kitimat fjord system: An introduction. In R. W. Macdonald (Ed.), *Proceedings of a workshop on the Kitimat marine environment, Canadian Technical Report of Hydrography and Ocean Sciences* (Vol. 18, pp. 2–13): Fisheries and Oceans Canada.

Mandelbrot, B. (1967). How long is the coast of Britain? statistical self-similarity and fractional dimension. *Science*, *156*(3775), 636–638.

Mandelbrot, B. B., & Van Ness, J. W. (1968). Fractional Brownian motions, fractional noises and applications. *SIAM review*, *10*(4), 422–437.

Molz, F., Liu, H., & Szulga, J. (1997). Fractional brownian motion and fractional gaussian noise in subsurface hydrology: A review, presentation of fundamental properties, and extensions. *Water Resources Research*, *33*(10), 2273–2286.

Nairn, B. J., & Kawase, M. (2002). Comparison of observed circulation patterns and numerical model predictions in Puget Sound, WA. In T. Droscher (Ed.), *Proc. 2001 Puget Sound Research Conference*. Olympia, WA: Puget Sound Water Quality Action Team.

Niiler, P. P., & Paduan, J. D. (1995). Wind-driven motions in the northeast Pacific as measured by Lagrangian drifters. *Journal of Physical Oceanography*, *25*(11), 2819–2830.

Niiler, P. P., Sybrandy, A. S., Bi, K., Poulain, P. M., & Bitterman, D. (1995). Measurements of the water-following capability of holey-sock and TRISTAR drifters. *Deep-Sea Research*, *42*(11/12), 1951–1964.

Okubo, A. (1971). Oceanic diffusion diagrams. *Deep-Sea Research*, *18*(8), 789–802.

Osborne, A. R., Kirwan, A. D., Provenzale, A., & Bergamasco, L. (1989). Fractal drifter trajectories in the Kuroshio extension. *Tellus A*, *41A*(5), 416–435.

Page, S. J., Hannah, C., Juhász, T., Spear, D., & Blanken, H. (2019). *Surface circulation tracking drifter data for the Kitimat Fjord system in northern British Columbia and adjacent continental shelf for April, 2014 to July, 2016*, Can. Data. Report. Hydrog. Ocean. Sci. 328: vi + 33pp.

Pawlowicz, R., Hannah, C., & Rosenberger, A. (2019). Lagrangian observations of estuarine residence times, dispersion, and trapping in the Salish Sea, estuarine. *Coastal and Shelf Science*, *225*, 106246.

Poje, A. C., Özgökmen, T. M., Lipphardt, B. Jr., Haus, B. K., Ryan, E. H., Haza, A. C., et al. (2014). Submesoscale dispersion in the vicinity of the Deepwater Horizon spill. *Proceedings of the National Academy of Sciences*, *111*(35), 12,693–12,698.

Poulain, P.-M., & Niiler, P. P. (1989). Statistical analysis if the surface circulation in the California current system using satellite-tracked drifters. *Journal of Physical Oceanography*, *19*, 1588–1603.

Rabe, B., & Hindson, J. (2017). Forcing mechanisms and hydrodynamics in Loch Linnhe, a dynamically wide Scottish estuary, Estuarine. *Coastal and Shelf Science*, *196*, 159–172.

Rabinovich, A. B., Krassovski, M. V., & Hannah, C. (2017). *Analysis of tidal currents in Douglas Channel*, Can. Tech. Rep. Hydrogr. Ocean Sci. 320: vi + 50pp.

Röhrs, J., & Christensen, K. H. (2015). Drift in the uppermost part of the ocean. *Geophysical Research Letters*, *42*, 10,349–10,356. https://doi.org/10.1002/2015GL066733

Röhrs, J., Christensen, K. H., Hole, L. R., Broström, G., Drivdal, M., & Sundby, S. (2012). Observation-based evaluation of surface wave effects on currents and trajectory forecasts. *Ocean Dynamics*, *62*, 1519–1533.

Röhrs, J., Christensen, K. H., Vikebø, F., Sundby, S., Saetra, Ø., & Broström, G. (2014). Wave induced transport and vertical mixing of pelagic eggs and larvae. *Limnology and Oceanography*, *59*(4), 1213–1227.

Rupolo, V., Artale, V., Hua, B. L., & Provenzale, A. (1996). Lagrangian velocity spectra at 700 m in the western North Atlantic. *Journal of Physical Oceanography*, *26*(8), 1591–1607.

Sanderson, B. G., & Booth, D. A. (1991). The fractal dimension of drifter trajectories and estimates of horizontal eddy-diffusivity. *Tellus*, *43A*, 334–349.

Sanderson, B. G., Goulding, A., & Okubo, A. (1990). The fractal dimension of relative lagrangian motion. *Tellus A*, *42*(5), 550–556.

Shan, S., Hannah, C. G., & Wu, Y. (2019). Coupling of estuarine circulations in a network of fjords. *Journal of Geophysical Research: Oceans*, *124*, 6809–6830. https://doi.org/10.1029/2018JC014924

Spencer, D., Lemckert, C., Yu, Y., Gustafson, J., Lee, S., & Zhang, H. (2014). Quantifying dispersion in an estuary: A Lagrangian drifter approach. *Journal of Coastal Research*, *70*, 29–34.

Spydell, M., Feddersen, F., & Guza, R. (2007). Observing surf-zone dispersion with drifters. *Journal of Physical Oceanography*, *37*, 2920–2939.

Spydell, M. S., Feddersen, F., Olabarrieta, M., Chen, J., Guza, R. T., Raubenheimer, B., & Elgar, S. (2015). Observed and modeled drifters at a tidal inlet. *Journal of Geophysical Research: Oceans*, *120*, 4825–4844. https://doi.org/10.1002/2014JC010541

St-Onge-Drouin, S., Winkler, G., Dumais, J.-F., & Senneville, S. (2014). Hydrodynamics and spatial separation between two clades of a copepod species complex. *Journal of Marine Systems*, *129*, 334–342.

Swick, W. A., & MacMahan, J. (2011). Field and numerical study on natural river mixing (Phd dissertation), Naval Postgraduate School, Monterey, California.

Taylor, G. (1921). Diffusion by continuous movements. *Proceedings of the Royal Society A*, *20*, 196–211.

Thomson, R. (1981). *Oceanography of the British Columbia coast*, Can. Spec. Publ. Fish. Aquat. Sci., pp. 291.

Thomson, R. E., & Emery, W. J. (2014). *Data analysis methods in physical oceanography* (3rd ed.). Amsterdam: Elsevier.

Tseng, R.-S. (2002). On the dispersion and diffusion near estuaries and around islands. *Estuarine Coastal and Shelf Science*, *54*, 89–100.

Valle-Levinson, A. (2008). Density-driven exchange flow in terms of the Kelvin and Ekman numbers. *Journal of Geophysical Research*, *113*, C04001. https://doi.org/10.1029/2007JC004144

Wan, D., Hannah, C. G., Foreman, M. G. G., & Dosso, S. (2017). Subtidal circulation in a deep-silled fjord: Douglas Channel, British Columbia. *Journal of Geophysical Research: Oceans*, *122*, 4163–4182. https://doi.org/10.1002/2016JC012022

Webster, I. (1980). Kitimat physical oceanographic study 1977-1978 part 3: Estuarine circulation (*Contract Report 80-3 (Part 3)*). Sidney, BC: Institute of Ocean Sciences.

Webster, I. (1983). The baroclinicity of the semi-diurnal tidal currents in Douglas Channel, B.C. In R. W. Macdonald (Ed.), *Proceedings of a workshop on the Kitimat marine environment, Canadian technical report of hydrography and ocean sciences* (Vol. 18, pp. 14–32). Sidney, BC: Fisheries and Oceans Canada.

Wessel, P., & Smith, W. H. F. (1996). A global, self-consistent, hierarchical, high-resolution shoreline database. *Journal of Geophysical Research*, *101*(B4), 8741–8743.

Wright, C., Vagle, S., Hannah, C., & Johannessen, S. (2015). *Physical, chemical and biological oceanographic data collected in Douglas Channel and the approaches to Kitimat, June 2013–July 2014*, Data. Report. Hydrog. Ocean. Sci. 196: viii + 66pp.

Wright, C., Vagle, S., Hannah, C., Johannessen, S., Spear, D., & Wan, D. (2016). *Physical, chemical and biological oceanographic data collected in Douglas Channel and the approaches to Kitimat, October 2014–July 2015*, Data. Report. Hydrog. Ocean. Sci. 200: viii + 74pp.

Wright, C., Vagle, S., Hannah, C., Johannessen, S., Spear, D., & Wan, D. (2017). *Physical, chemical and biological oceanographic data collected in Douglas Channel and the approaches to Kitimat, October 2015–July 2016*, Data. Report. Hydrog. Ocean. Sci. 202: x + 139pp.